ISSN 0915-633X

NATIONAL INSTITUTE FOR FUSION SCIENCE

Loss Cone Region in Toroidal Helical Systems

K. Itoh, H. Sanuki, J. Todoroki, T. Kamimura, S.-I. Itoh,
A. Fukuyama and K. Hanatani

(Received – Dec. 11, 1989)

NIFS-13 Feb. 1990

RESEARCH REPORT
NIFS Series

NAGOYA, JAPAN

Loss Cone Region in Toroidal Helical Systems

K. Itoh, H. Sanuki, J. Todoroki, T. Kamimura, S.-I. Itoh

National Institute for Fusion Science, Furo-cho, Chikusa-ku,
Nagoya, 464-01,

A. Fukuyama

Faculty of Engineering, Okayama University, Okayama 700,

and

K. Hanatani

Plasma Physics Laboratory, Kyoto University
Gokasho, Uji 611

Keywords: Loss Cone, Helical Systems, Particle Orbit, Absolute Trapping

Abstract

Analytic formula is derived for the loss cone in the toroidal helical systems. Particular emphasis is put on the loss region for the particles which are barely trapped in the helical ripples. Effects of the radial electric field and shifts of the magnetic axis are discussed. Loss region is shown to be much wider than the evaluation given for the deeply trapped particles.

§1. Introduction

The evaluation of the loss cone in toroidal helical systems is inevitable in studying the potential applicability for the reactor[1-10]. The loss cone problem would be serious for the alpha particles which are generated by nuclear fusion reaction. The absolute trapping of particle has attracted wide attentions recently[7-11]. This is partly because the system with low toroidal pitch number m, which is usually considered to have wide loss cone, has been shown to have high MHD β limit.[12-14] The study on the particle trapping has also been flourished because the method of improvements such as the shift of toroidal axis have been proposed. It has also been pointed out long time that the radial electric field has also considerable effect on the particle trapping[3]. Lots of calculation has been performed, particularly for the ℓ=2 torsatron/helical-heliotron configurations[15], to identify the loss region in the velocity as well as the real spaces. (ℓ is the multipolarity of the field.) An analytic formula of the loss region has been derived in the presence of the radial electric field for the deeply trapped particles[9]. The formula has been applied to evaluate the consistent radial electric field. It is well known, however, the loss region for the deeply trapped particles only describe the lower limit of the loss region. Much wider loss region has been known for the barely trapped particles. In order to have the analytic insight as well as to combine the analysis on the loss cone with more complicated calculation such as the transport, an analytic

formula is still required for the loss cone.

In this article, we extend the previous analysis[9] on the loss cone to the more general case, and derive a simple analytic formula for the loss region for the barely trapped particles. The effect of the radial electric field and the role of the shift of the toroidal axis are studied. Effect of the nonuniform E×B rotation is also discussed. We confirm that much larger inward shift of axis is required to eliminate the loss cone from the core plasma for barely trapped particles compared to the deeply trapped particles. Upper limit of the ratio of the toroidal ripple to the helical ripple is also found. This would impose severer limit for the compatibility with the high MHD β-limit. The minimum energy of particles to enter the loss cone is studied in the presence of the radial electeric field. If the direction of the field is inward, i.e., the E×B rotation cancels the ∇-B drift of ions, the ion confinement is detereorated. The result shows small difference from the previous calculation on the deeply trapped particles.

§2. Model of Loss Cone

§2.1 Trajectory of the Guding Center of the Banana Orbit

We study a toroidal helical configuration with $\ell=2$. The geometry of the configuration is shown in Fig.1. An example of the particle orbit is shown in Fig.1 projected on the poloidal cross section. Toroidal coordinates (r,θ,ζ) are used, where θ and ζ are poloidal and toroidal angles, respectively, R is the major radius of the torus and a is the minor radius. The deviation of the guiding center of the banana orbit from the magnetic surface is much larger than the banana width itself. We therefore study in this article the trajectory of the guiding center of the banana orbit in order to calculate the loss cone boundary.

The motion of the guding center is predicted by the J-invariance of the orbit. The J-invariance for the trapped particle is defined as

$$J \equiv \frac{1}{2\pi} \oint d\ell \, \frac{v_{//}}{B} \, d\zeta \ , \tag{1}$$

where $v_{//}$ is the velocity component parallel to the magnetic field. We choose a model magnetic field as

$$B = B_0\{1 - \varepsilon_t(r)\cos\theta - \tilde{\varepsilon}_h(r,\theta)\cos(2\theta - m\zeta)\} \ , \tag{2}$$

where $\varepsilon_h(r,\theta)$ is given as

$$\tilde{\varepsilon}_h(r,\theta) = \varepsilon_{ha}[(r-\Delta\cos\theta)^2 + \Delta^2\sin^2\theta] \ . \qquad (3)$$

The quantities $\varepsilon_t(r)$ and $\tilde{\varepsilon}_h(r,\theta)$ represent toroidal and helical ripples, respectively. The model implies that the magnitude of the helical ripple depends on the distance from the geometrical center, from which the magnetic axis is shifted by the amount of Δ. If Δ is positive, the axis is shifted inward. We here simply assume that the shift parameter Δ does not affect the shape of $\tilde{\varepsilon}_h$ nor the plasma minor radius a. If one applies the following analysis to a real configuration, the relation between the shift and parameters a and Δ must be employed in an explicit form. We also assume that the static potential is constant on the magnetic surface and is given as $\phi(r)$.

The J-invariance is given as

$$J = \frac{2}{m}R\sqrt{\frac{\mu B_0}{M}}\sqrt{\tilde{\varepsilon}_h}\,F(\kappa^2), \qquad (4)$$

where

$$F(\kappa^2) = \frac{4}{\pi}\{E(\kappa)-(1-\kappa^2)K(\kappa)\} \qquad (5)$$

and

$$\kappa^2 = \frac{W - \mu B_0\{1-\varepsilon_t(r)\cos\vartheta-\tilde{\varepsilon}_h(r,\theta)\} - q\phi}{2\tilde{\varepsilon}_h\mu B_0}, \qquad (6)$$

where B is the magnetic field, m is the toroidal pitch, μ is the magnetic moment, W is the particle energy, M is the mass and q is the charge. The functions K and E stand for the complete elliptic integrals of the first kind and the second kind, respectively.

The equations (4) and (6) yield two constant of motion, i.e.,

$$\hat{J} = \sqrt{\tilde{\varepsilon}_h}\, F(\kappa^2) \tag{7}$$

and

$$\frac{W}{\mu B_0} - 1 = (2\kappa^2-1)\tilde{\varepsilon}_h(r,\theta) - \varepsilon_t(r)\cos\theta + \frac{q\phi}{\varepsilon_h \mu B_0} . \tag{8}$$

The guiding center motion has two invariances J and $W/\mu B_0$. By eliminating κ^2 from Eqs.(7) and (8), we have the integral of motion for the trapped particles. The equation (7) and (8) contain the elliptic integral and requires numerical solution. One limit to allow the analytic treatment is $\kappa=0$, i.e., the study on the deeply trapped particles. Taking the Taylor expansion of the elliptic integrals, we here derive the approximate formula for the barely trapped particles. The function F is expanded as

$$F(\kappa^2) = \kappa^2 \{1 + \frac{1}{8}\kappa^2 + \frac{3}{64}\kappa^4 + \cdots\} . \tag{9}$$

Taking the first order correction with respect to κ^2, Mynick classifies the trapped particle orbits[8]. Replacing F by κ^2 in Eqs.(7) and (8), we have the constant of motion as

$$\psi(r,\theta) = \psi_0(r,\theta) + \psi_1(r)\cos\theta \equiv 1 - \frac{W}{\mu B_0} , \qquad (10)$$

with

$$\psi_0(r,\theta) = [\sqrt{\tilde{\varepsilon}_h(r,\theta)} - \kappa_1^2\sqrt{\tilde{\varepsilon}_h(r_1,\theta_1)}]^2 - \kappa_1^4\tilde{\varepsilon}_h(r_1,\theta_1) - \frac{q\phi}{\mu B_0} , \qquad (11\text{-}1)$$

$$\psi_1(r) = \varepsilon_t(r) , \qquad (11\text{-}2)$$

and the electrostatic potential is given as

$$\phi(r) = \phi_0 f(r) , \qquad (12)$$

where $f(r)$ satisfies that $f(0)=0$ and $f(1)=1$. The position (r, θ) of the particle which starts from $(r_1, \theta_1, \kappa_1)$ satisfies the relation Eq.(10).

The integral provides the basis to calculate the loss cone region. In the following subsections §2.2 and §2.3, we choose the case of uniform E×B rotation (i.e., f is parabolic). The case of nonuniform E×B rotation is discussed in §2.4.

§2.2 Region of the Loss Cone for Helically Trapped Particle

We calculate the loss region on the mid-plane for the helically trapped particles. The loss condition is defined such that the particles are assumed to be lost if r reaches a. The plausibility of this choice of the loss boundary is discussed in §4.

The loss cone is determined by calculating the largest orbit

which does not across the boundary r=a. The largest contained orbit which has the pitch angle parameter κ_1^2 on the mid-plane is determined by

$$r=a \ (\theta=\pi) \text{ and } \kappa=\kappa_1 \ (\theta=0) \tag{13}$$

if $\partial\psi_0/\partial r>0$ at r=a, i.e., the orbits shift inward as is shown in Fig.2(a). In other case, the condition

$$r=a \ (\theta=0) \text{ and } \kappa=\kappa_1 \ (\theta=\pi), \tag{14}$$

determines the loss boundary, if $\partial\psi_0/\partial r<0$ at r=a. In this case the orbit shifts outward (i.e., the large ExB rotation reverses the drift). In the following, we study the loss cone of ions by choosing q=e. The results for electrons are obtained only by changing the sign of e. This simplification is possible by neglecting the banana width in comparison with the deviation of the banana center from the magnetic surface.

The relations (10) and (13) (or (14)) give the equation which dictates the loss boundary. Equation (7) can be written as

$$F(\kappa^2) = \frac{x-\hat{\Delta}}{1+\hat{\Delta}} \ F(\kappa_1^2) \tag{15}$$

and the constant of motion $\psi(a,\pi,\kappa)=\psi(r_{boundary},0,\kappa_1)$ is reduced to

$$(2\kappa^2-1)\varepsilon_{ha}(1+\hat{\Delta})^2+\varepsilon_t(a) + \frac{e\phi_0}{\mu B_0}$$
$$= (2\kappa_1^2-1)\varepsilon_{ha}(x-\hat{\Delta})^2-\varepsilon_t(a)x + \frac{e\phi_0}{\mu B_0}x^2 , \qquad (16)$$

where $x=r_{boundary}/a$, $r_{boundary}$ is the minor radius, out of which the loss cone exist in the phase space, and $\hat{\Delta}$ is Δ/a.

Taking the first order correction of κ^2 on F and replacing F by κ^2 in Eq.(7), we have

$$\frac{e\phi_0}{\varepsilon_{ha}\mu B_0} = \frac{\{1+x+2(\hat{\Delta}-x)\kappa_1^2\}(1+2\hat{\Delta}-x)-\varepsilon(1+x)}{1-x^2} \qquad (17)$$

for the loss boundary, where $\varepsilon=\varepsilon_t(a)/\varepsilon_{ha}$. Equation (17) shows that the loss boundary $r_{boundary}$ is smallest for $\kappa_1=1$, i.e., barely trapped particles. For instance, Eq.(17) reduces to

$$\kappa_1^2 = \frac{1+x}{2x-2\hat{\Delta}}\{1 - \frac{\varepsilon}{1+2\hat{\Delta}-x}\} \qquad (18)$$

in the absence of the electric potential. The value $\bar{x}$ is minimum for $\kappa_1^2=1$ as

$$\bar{x} = 1 + 2\hat{\Delta} + \frac{\varepsilon}{2} - \sqrt{\frac{\varepsilon^2}{4}+2(1+\hat{\Delta})\varepsilon} . \qquad (19)$$

If the electric field is so strong that the ExB rotation reverses the poloidal drift, Eq.(14) determines the loss cone boundary. With the same procedure, Eq.(14) can be simplified as

$$\frac{e\phi_0}{\varepsilon_{ha}\mu B_0} = \frac{\{1+x-2(\hat{\Delta}+x)\kappa_1^2\}(1-2\hat{\Delta}-x) + \varepsilon(1+x)}{1-x^2} . \qquad (20)$$

Combining Eqs.(17) and (20), we have the loss region for the barely trapped particles as

$$\Phi_1 < \Phi_0 < \Phi_2 \tag{21}$$

and

$$\frac{e\phi_1}{\varepsilon_{ha}\mu B_0} = \frac{(1+2\hat{\Delta}-x)^2}{1-x^2} - \frac{\varepsilon}{1-x} \quad , \tag{22-1}$$

$$\frac{e\phi_2}{\varepsilon_{ha}\mu B_0} = \frac{(1-2\hat{\Delta}-x)^2}{1-x^2} + \frac{\varepsilon}{1-x} \quad . \tag{22-2}$$

We compare the result with the case for deeply trapped particles. Substituting $\kappa_1^2=0$ into Eqs.(17) and (20), we have

$$\frac{e\phi_1}{\varepsilon_{ha}\mu B_0} = 1 + \frac{2\hat{\Delta}}{1-x} - \frac{\varepsilon}{1-x} \quad , \tag{23-1}$$

$$\frac{e\phi_2}{\varepsilon_{ha}\mu B_0} = 1 - \frac{2\hat{\Delta}}{1-x} + \frac{\varepsilon}{1-x} \quad , \tag{23-2}$$

for deeply trapped particles. Equation (22-1) shows that the loss cone boundary is much wider, i.e., closer to the magnetic axis, for the barely trapped particles. If the electric field is strongly negative and the poloidal drift of ions is reversed, then the loss region is wider for the deeply trapped particles. This is because the ∇B-drift is larger for smaller values of κ^2 and the total poloidal drift remains smaller for given values of

particle energy and E_r.

§2.3 Loss Boundary for Transition Particle

Equations (19) and (22-1) show that the barely trapped particles are easily lost. We next study the loss cone boundary for the particles which experience the transition between helically trapped and transit orbits. We introduce the poloidal angle θ_1 at which $\kappa^2=1$ is satisfied; in the region $|\theta|<\theta_1$, the particle moves as a transit particle, and turns to be a trapped one at $\theta=\theta_1$. The loss boundary is determined by the relation

$$r=a \ (\theta=\pi) \text{ and } \kappa_1=1 \ (\theta=\theta_1, \ r=r_{boundary}) \tag{24}$$

if the orbits shift inward. Instead of Eqs.(15) and (16), we have

$$F(\kappa^2) = \frac{\sqrt{(x-\hat{\Delta}\cos\theta_1)^2+\hat{\Delta}^2\sin^2\theta_1}}{1+\hat{\Delta}} F(1) \tag{25}$$

and

$$\begin{aligned}&(2\kappa^2-1)(1+\hat{\Delta})^2 + \varepsilon + \frac{e\phi_0}{\varepsilon_{ha}\mu B_0} = \\ &(x-\hat{\Delta}\cos\theta_1)^2+\hat{\Delta}^2\sin^2\theta_1 - \varepsilon x\cos\theta_1 + \frac{e\phi_0\, x^2}{\varepsilon_{ha}\mu B_0} \ .\end{aligned} \tag{26}$$

This result shows that the reduction of the loss cone loss by inward shift of the magnetic axis is smaller for the transition particles compared to helically trapped particles. For instance,

if we take $\phi = 0$ for the simplicity, we have

$$\{\sqrt{(x-\hat{\Delta}\cos\theta_1)^2+\hat{\Delta}^2\sin^2\theta_1} - 1 - \hat{\Delta}\}^2 - \varepsilon(1+x\cos\theta_1) = 0. \quad (27)$$

The loss boundary x is minimum for barely trapped particles, $\kappa_1^2 = 1$ at $\theta_1=0$, in the absence of the inward shift Δ. However, the loss cone of the transition particles becomes important if the inward shift of the axis increases. The effect of the shift becomes small for finite value of θ_1, and disappears for $\theta_1=\pi$. This means that the loss cone cannot be annihilated in the region

$$r/a > 1 - \varepsilon_t(a)/\varepsilon_h(a) \quad (28)$$

even by the shift of the magnetic axis.

§2.4 Nonuniform E×B Rotation

If the profile of f(r) differs from the parabolic one, the loss cone condition is modified from those in §2.2 and §2.3. The modification is considerable if the resonance condition $\partial\psi_0/\partial r=0$ is satisfied in the plasma. If the resonance condition is not caused by the nonuniformity of E×B rotation, however, there appears no qualitative change. The loss cone boundary is obtained only by replacing the term $(1-x^2)$ by $(1-f(x))$ in the denominator of Eq.(22) as

$$\frac{e\phi_1}{\varepsilon_{ha}\mu B_0} = \frac{(1+2\hat{\Delta}-x)^2 - \varepsilon}{1-f(x)}, \quad (29\text{-}1)$$

$$\frac{e\phi_2}{\varepsilon_{ha}\mu B_0} = \frac{(1-2\hat{\Delta}-x)^2+\varepsilon}{1-f(x)} \quad . \tag{29-2}$$

If, on the other hand, the resonance surface appears in the plasma column so that the relation (neglecting $\hat{\Delta}$)

$$\psi_0'(r) = 0 \qquad \text{at } r=r_s \tag{30}$$

holds, the orbit topology changes. We study the case of $\psi'(0)>0$ and $\psi'(a)<0$ (prime denotes the derivative with respect to r). The opposite case is given by straightforward extension. We define the radius r_2 by the relation $\psi''(r_2)=0$. If the toroidicity is weak and the toroidal ripple is small, such that

$$\varepsilon_t(a) < \psi_0'(r_2) \tag{32}$$

holds, then there appears a separatrix in constant ψ surfaces. The width of the island in the constant ψ surfaces is estimated as

$$\delta r \sim 2\sqrt{\frac{\varepsilon_t(r_1)}{|\psi_0''(r_1)|}} \tag{33}$$

On the other hand, if the toroidal ripple is large, i.e.,

$$\varepsilon_t(a) > \psi_0'(r_2) \ , \tag{34}$$

the constant ψ surfaces are nested and kidney bean shaped.

The loss cone region is calculated by using the integral Eq.(10). Substituting r=a and θ=0 into Eq.(10), the loss cone boundary is given as a function of κ_1 for given functional form of f(r). Figure 3 shows the loss cone region schematically on the r-θ plane for small and large ε cases. In the weak ε case, where Eq.(32) holds, the topology of the loss cone region depends on the magnitude of $\varepsilon=\varepsilon_t(a)/\varepsilon_{ha}$. When δr is smaller than $a-r_s$, the loss cone region is outside of the island, satisfying the relation $x > r_s/a$. If δr becomes larger than $a-r_s$, then the loss cone region penetrates into the core.

§3 Comparison with Numerical Calculation

The result is compared to numerical calculation in order to see the plausibility of the analytic formula.

Figures 4 and 5 show the loss boundary in r/a-pitch angle plane and in r/a-ϕ_0 plane, respectively. The model of ε_h, ε_t, Δ and ϕ in numerical calculation is the same as for the analytic calculation. Electrostatic potential profile is chosen as parabolic, $f(r)=(r/a)^2$. Figure 4 shows the κ_1 effect on the loss cone and Fig. 5 illustrates the effect of the radial electric field. The solid line in Fig.4 is the analytic formula

$$\frac{W_{//}(\theta=0)}{\varepsilon_{ha}\mu B_0} = \frac{x(1+x)(1-x-\varepsilon)}{1-x} \quad . \tag{35}$$

In Fig. 5, analytic formula

$$\frac{e\phi_0}{\varepsilon_{ha}\mu B_0} = \frac{1-x}{1+x} \mp \frac{\varepsilon}{1-x} \tag{36}$$

(minus and plus sign corresponds to solid and dashed lines, respectively) are compared to numerical calculation. The open circles indicate the result of the numerical calculation[11]. The small difference comes from partly because we only keep the first order correction of κ^2 in Eq.(9) and partly because the finite banana width in numerical calculation further reduces the confined region. The error in evaluating x is less than 5% for standard parameters. In order to illustrate that the barely trapped particles are hardly confined compared to deeply trapped

particles, we show the loss boundary for deeply trapped particles in Fig. 5 by solid circles. The dashed line denotes the analytic formula Eq.(23-1), which gives a better agreement. From this result we see that the formula Eq.(22-2) gives an upper bound for the confined region.

The magnetic axis shift reduces the loss region[7-11]. Figure 6 compares the loss boundary for analytic and numerical calculations. The open circles are the result of numerical calculation[11] and solid curve is given from Eq.(22-1) with $\Phi_0=0$. The effect of the axis shift on the loss boundary, i.e., $\partial r_{boundary}/\partial\Delta$, shows a good agreement between them. The boundary for the deeply trapped particles is also shown in Fig.6 for the comparison. The axis shift for the barely trapped particles is as effective as for deeply trapped particles. However, the annihilation of the loss cone is far difficult for the barely trapped particles. The result for the transition particle is shown in Fig.7. As Δ is small, the loss cone is largest for the barely trapped particles. However, the minimum value of x is given by the transition particles when Δ becomes large enough as is shown by numerical computation. If one intends to annihilate the loss cone within the region of a half radius, i.e., $r_{boundary}/a=1/2$, one must have

$$\hat{\Delta} > \sqrt{\frac{3\varepsilon}{8}} - \frac{1}{4} \qquad \text{(barely trapped)} \qquad (37\text{-}1)$$

$$\left.\begin{aligned} &\hat{\Delta} > \frac{1}{8(1-\sqrt{\varepsilon})} - \frac{1-\sqrt{\varepsilon}}{2} \quad (\theta_1 = \tfrac{\pi}{2}) \\ &\varepsilon < \frac{1}{2} \qquad\qquad\qquad\qquad (\theta_1 = \pi) \end{aligned}\right\} \text{(transition)} \qquad (37\text{-}2)$$

in stead of

$$\hat{\Delta} > \frac{\varepsilon}{2} - \frac{1}{4} . \qquad \text{(deeply trapped)} \qquad (38)$$

When the direction of the electric field is inward, $E_r<0$, the confinement of ions depends on the E×B rotation. The energetic particles are lost through the resonance of E×B rotation and ∇B drift. The upper bound of the energy of confined particles are given by Eq.(22-2). This energy boundary is important in determining the self-consistent electric field in the presence of the loss cone loss[9]. Figure 8 shows the loss region in the r/a-pitch-angle space under the condition of negative electric field. The loss cone is widest for the deeply trapped particles as is seen from Eqs.(22-2) and (23-2). The analysis on the self-consistent electric field by using the formula of deeply trapped particles still provide a valid estimation even if one includes the effect of the barely trapped particles.

§4 Summary and Discussion

In this article, we derived an analytic formula of the loss boundary in the real and phase spaces in the toroidal helical systems. By using the J-invariance of the trapped particles, the loss boundary for the deeply trapped particles was studied. The Taylor expansion of the function F permitted the analytic estimation of the loss cone region. The formula was derived in the limit of zero poloidal gyroradius. The effect of the radial electric field and the shift of the magnetic axis were studied. The effect of the nonuniform E×B rotation is also investigated. It is confirmed that the annihilation of the loss cone from the core plasma is far difficult compared to the deeply trapped particles. The formula for the transition particle was also derived. The loss cone of such particles is not so sensitive to the shift of the magnetic axis compared to deeply trapped particles. The ratio $\varepsilon_t(a)/\varepsilon_h(a)$ must be small enough to reduce the loss cone.

The analysis in this article is given in the limit of small poloidal gyroradius. If one take into account the finite poloidal gyroradius effect, the loss boundary $r_{boundary}$ become smaller by the amount of the order of the poloidal gyroradius.

The formula was compared to the numerical calculations. The difference of $r_{boundary}$ normalized to a is less than 5% for standard parameters. The simple formula will allow the analytic insight for the parameter dependence of the loss boundary as well

as the rapid calculation for the more complicated calculations such as the transport code analysis.

In order to keep the simplicity of the formula, only the first order correction is taken into account. If one keeps higher order correction, better estimates are obtained. The second order correction gives (in case of $\Delta=0$ for example)

$$\frac{e\phi_0}{\varepsilon_{ha}\mu B_0} = \left[\frac{1-x}{1+x} - \frac{\varepsilon}{1-x} \right] - \frac{x}{8(1+x)} \qquad (39)$$

instead of Eq.(22-1) for the loss boundary. The symbol $\times$ in Fig.6 shows the result of Eq.(39) for the case of $\Delta=0$. We see better agreement, the accuracy of which is about 1%.

In studying the actual confining configurations, the form of $\varepsilon_h(r,\theta)$ is not always as simple as in this article. The inward shift of the axis in experiments would cause changes in a and higher harmonics of ε_h. Quantitative conclusion for the loss cone boundary requires calculations on the real geometry; This kind of the analytic formula, however, is useful to understand the trends which is observed in numerical computation and to study more complex problems such as the determination of the selfconsistent radial electric field in the presence of the loss cone.

We finally note the choice of the plasma boundary. The larger choice of the limiter radius gives a wider confined region, in principle. However, the minimum energy of the confined particles only slightly depends on the choice of the limiter boundary in the presence of negative electric field,

which sets the severe loss boundary. For instance, the minimum energy of confinement at r=0 does not depend on the limiter radius. It is also noted that the particles drifting close to the surface are subject to strong Coulomb collision with cold electrons or to the charge exchange loss with neutral particles. Owing to these reasons, we choose the plasma surface to determine the loss cone boundary.

Acknowledgements

One of the authors (KI) acknowledges the discussion with Dr. H. Zushi. Continuous encouragements by Dr. A. Iiyoshi is also acknowledged. This work is partly supported by the Grant-in-Aid for Fusion Research of MoE Japan.

References

[1] A. Gibson, J. B. Taylor, Phys. Fluids 10 (1967) 2653.

[2] A.A. Galeev, R. Z. Sagdeev, H. P. Furth, M. N. Rosenbruth, Phys. Rev. Lett. 22 (1969) 511.

[3] H. P. Furth, M. N. Rosenbluth, in Plasma Physics and Controlled Nuclear Fusion Research (Proc. 3rd Int. Conf. 1968) Vol.1, IAEA, Vienna (1969) 821.

[4] D. Dobrott, E. A. Freeman, Phys. Fluids 14 (1971) 349.

[5] K. Miyamoto, Nucl. Fusion 18 (1978) 243.

[6] M. Wakatani, S. Kodama, N. Nakasuga, K. Hanatani, Nucl. Fusion 21 (1981) 175.

[7] H. E. Mynick, T. K. Chu, A. Boozer, Phys. Rev. Lett. 48 (1982) 322.

[8] H. E. Mynick, Phys. Fluids 26 (1983) 1008.

[9] K. Itoh, S.-I. Itoh, A. Fukuyama, K. Hanatani, Nucl. Fusion 29 (1989) 1851.

[10] B. A. Carreras, N. Dominguez, L. Garcia, V. E. Lynch, J. F. Lyon, Nucl. Fusion 28 (1988) 1195.

[11] H. Sanuki, J. Todoroki, T. Kamimura, submitted to Phys. Fluids.

[12] B. A. Carreras, H. R. Hicks, J. A. Holmes, V. E. Lynch, Phys. Fluids 26 (1983) 3569.

[13] J. Todoroki, T. Kamimura, H. Sanuki, T. Amano, T. Hayashi, et al., in 12th International Conference on Plasma Physics and Controlled Nuclear Fusion Research (IAEA, Nice, 1988) paper IAEA-CN-50/C-5-4.

[14] Y. Nakamura, K. Ichiguchi, M. Wakatani, J. L. Johnson, J. Phys. Soc. Jpn. 58 (1989) 3157.

[15] C. Gourdon, D. Marty, E. K. Maschke, J. P. Dumont, in Plasma Physics and Controlled Nuclear Fusion Research (Proc. 3rd Int. Conf. 1968) Vol.1, IAEA, Vienna (1969) 847.

Figure Captions

Fig.1 (a) Geometry of the analysis. (b) Poloidal cross-sections of the magnetic surface and mod-B surface at $\zeta=0$. (c) Example of the particle orbit on the r-ϑ plane. The banana center has a circular movement.

Fig.2 Trajectory of banana center which determines the loss cone boundary. Helically trapped particles (a) and transition particles (b). The outer circle is given by $r=a$. (schematic drawing)

Fig.3 Orbit of banana center in the presence of the resonance surface due to the nonuniform ExB rotation is shown schematically. Cases of weak toroidicity, Eq.(32), (a, b) and strong toroidicity, Eq.(34), (c). Separatrix width δ is smaller than $a-r_s$ in (a), and is larger than $a-r_s$ in (b). $\psi_0'(r_s)=0$ holds and r_b is the radius of the confined region. Shaded areas denote the loss region.

Fig.4 The loss cone boundary for helically trapped particle. L and C denotes the loss and confined regions, respectively. Thick solid line is the result of the analytic formula, and the dashed line is the result of the numelical computation. dashed-dotted line indicate

the boundary of helically trapped particle at $\theta=0$. Parameters are $\varepsilon_t(a)=0.11$, $\varepsilon_h(a)=0.24$, $\phi_0=0$ and $\Delta=0$.

Fig.5 The loss cone boundary for helically trapped particles in the presence of the radial electric field. Solid lines are the result of the barely trapped aprticles ($\kappa^2=1$ on the midplane), and dashed lines are for the deeply trapped particles ($\kappa^2=0$ on the midplane). Circles denotes the result of numerical computation. Parameters are the same as in Fig.3. For thin dashed line, see Eq.(39).

Fig.6 Effect of the magnetic axis shift on the loss cone boundary. Solid lines are for barely trapped particles and dashed lines are deeply trapped aprticles. Parameters are the same as in Fig.3. The simbol $\times$ indicates the result with higher order correction, Eq.(26). Open circles show the result of numerical calculation.

Fig.7 Loss boundary of transition particles in the presence of the magnetic axis shift ($\theta_1=\pi$ and $\pi/2$). Result of barely trapped particle is also shown by dashed line. Parameters are the same as in Fig.3.

Fig.8 Loss cone boundary in the presence of negative electric field. Solid line denotes the result of the analysis and the dashed line is given by the numerical

calculation. $\Phi_0/W=0.4$ and other parameters are the same as in Fig.3.

Fig. 1(a)

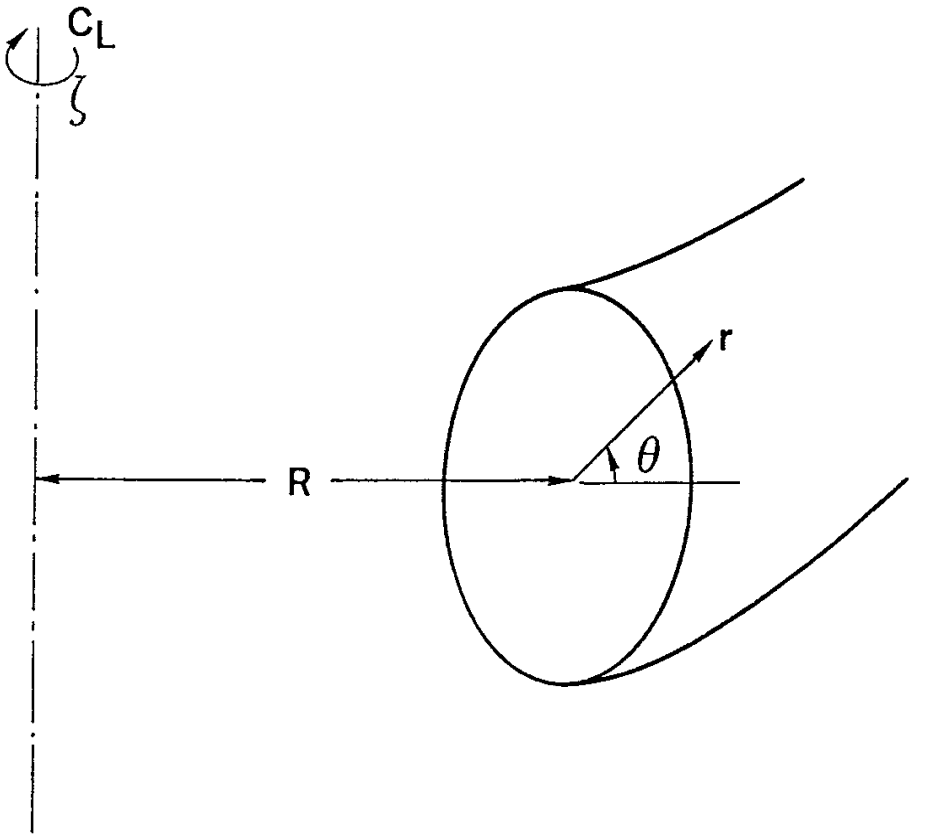

Fig. 1(b)

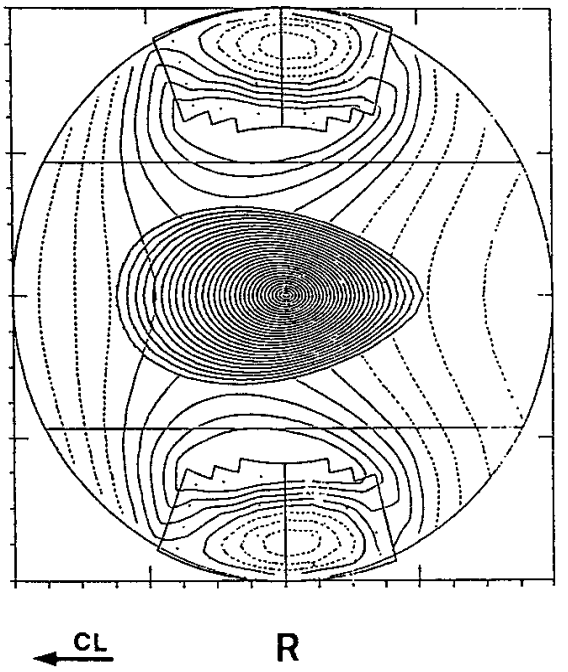

Fig. 1(c)

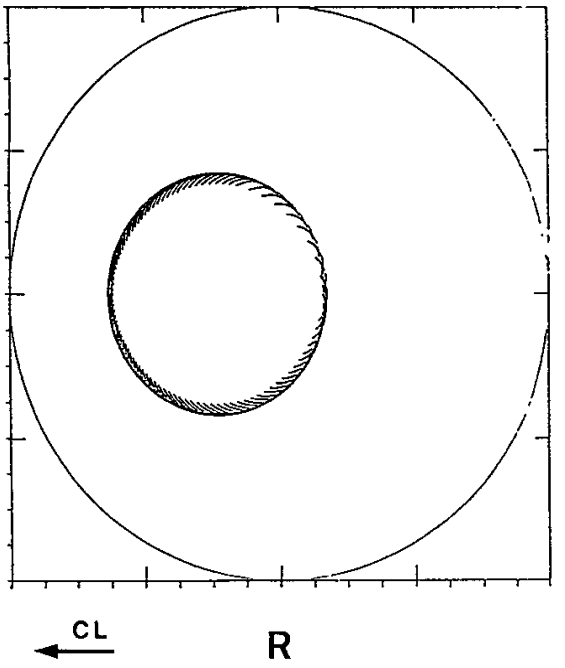

Fig. 2

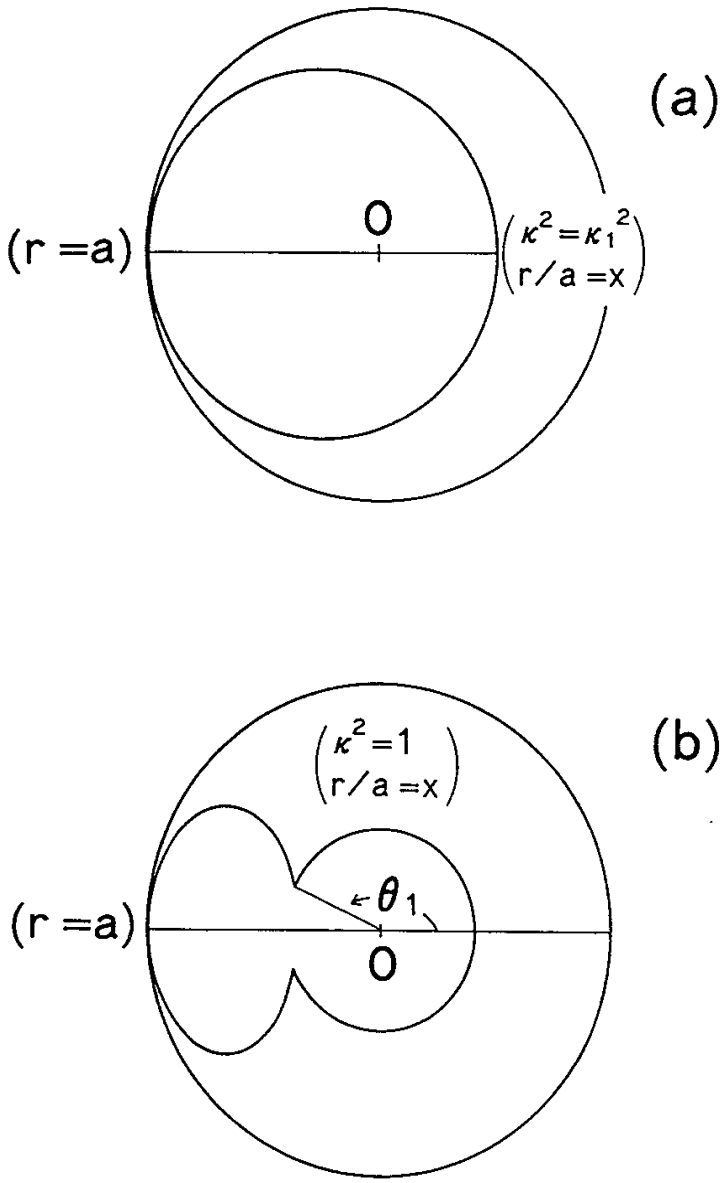

Fig. 3

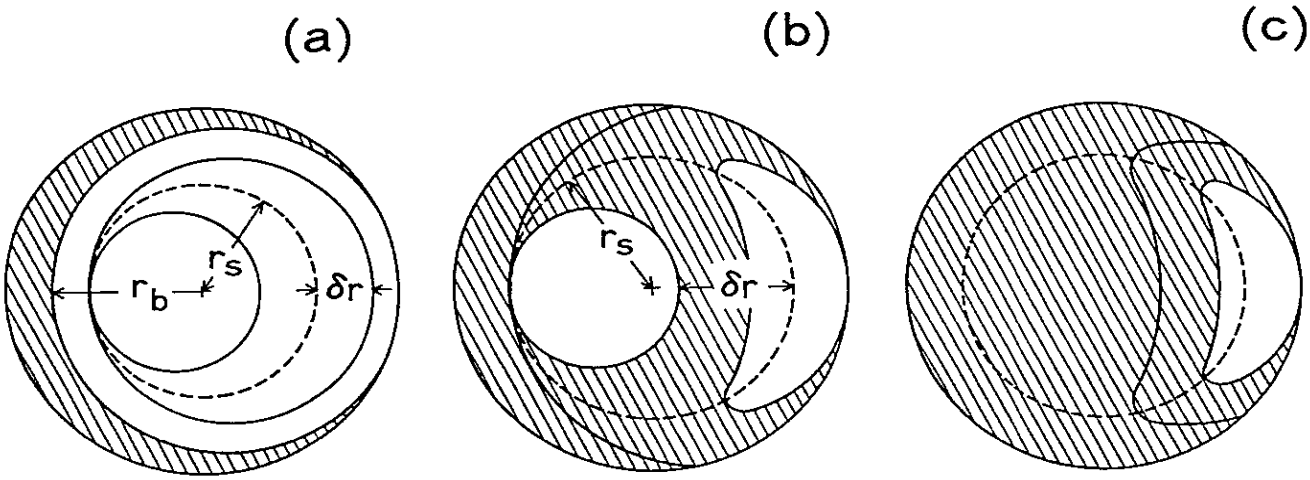

Fig. 4

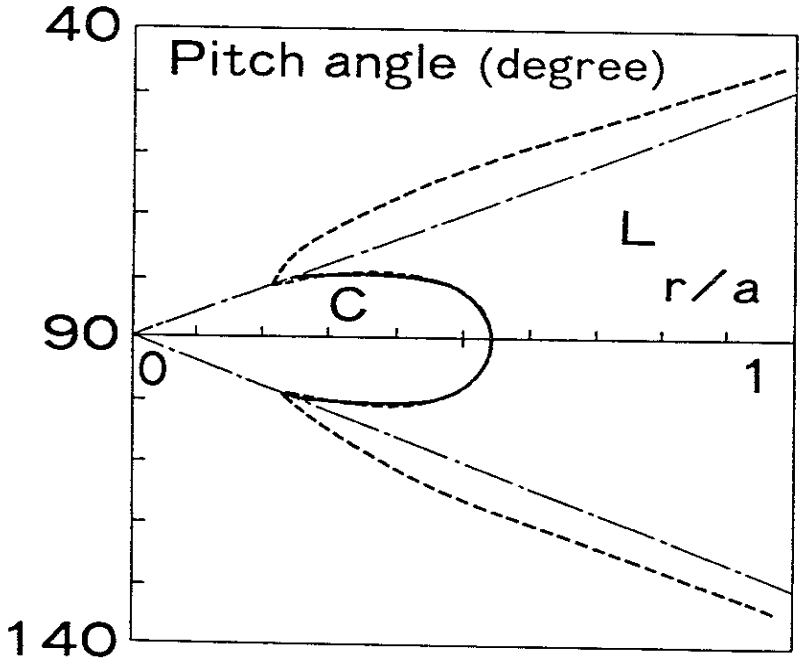

Fig. 5

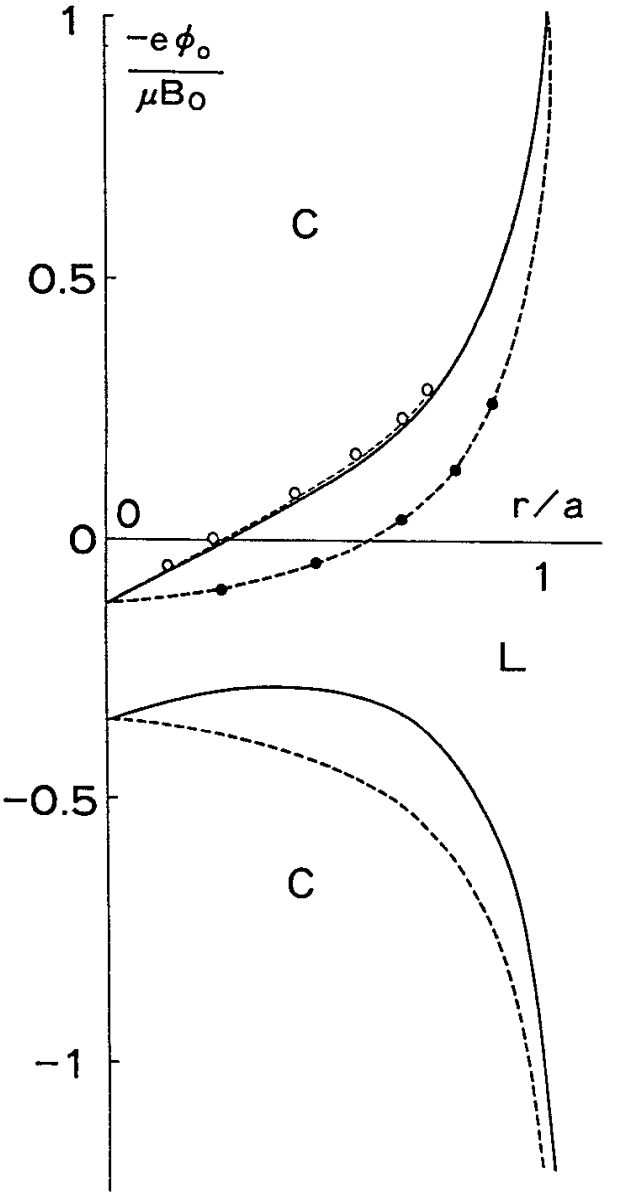

Fig. 6

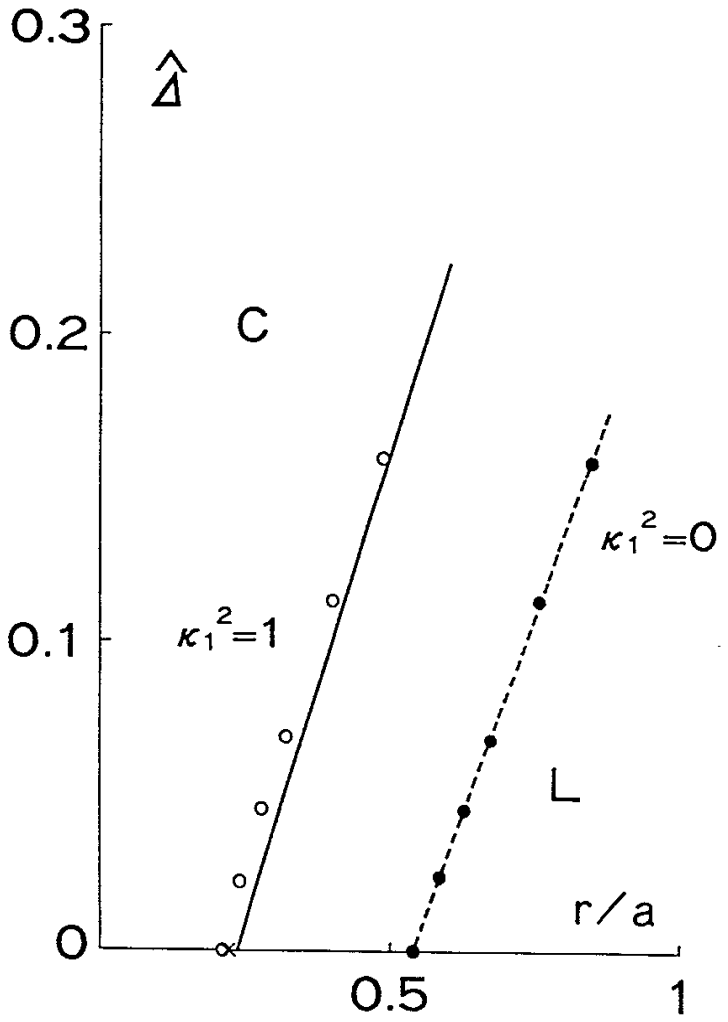

Fig. 7

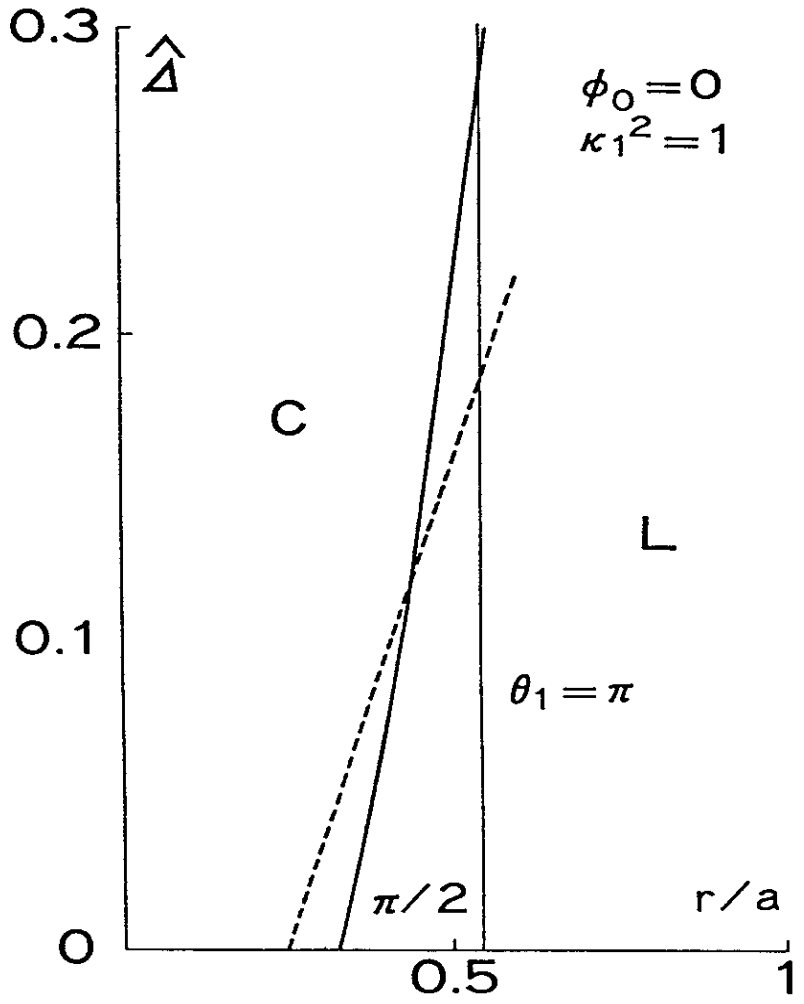

Fig. 8